ISSN 0915-633X

NATIONAL INSTITUTE FOR FUSION SCIENCE

Behavior of Pellet Injected Li Ions into Heliotron E Plasmas

K. Kondo, K. Ida, C. Christou, V.Yu.Sergeev, K.V. Khlopenkov, S.Sudo, F. Sano, H. Zushi, T. Mizuuchi, S. Besshou, H. Okada, K. Nagasaki, K. Sakamoto, Y. Kurimoto, H. Funaba, T. Hamada, T. Kinoshita, S. Kado, Y. Kanda, T. Okamoto, M. Wakatani and T. Obiki

(Received - June 5, 1996)

NIFS-421 July 1996

RESEARCH REPORT
NIFS Series

NAGOYA, JAPAN

Behavior of Pellet Injected Li Ions into Heliotron E Plasmas

K.Kondo[1)], K.Ida[3)], C.Christou[1)], V.Yu.Sergeev[4)], K.V.Khlopenkov[4)], S.Sudo[3)], F.Sano[2)], H.Zushi[1)], T.Mizuuchi[2)],S.Besshou[1)], H.Okada[2)], K.Nagasaki[2)], K.Sakamoto[2)], Y.Kurimoto[5)], H.Funaba[5)], T.Hamada[5)], T.Kinoshita[5)], S.Kado[6)], Y.Kanda[5)], T.Okamoto[5)], M.Wakatani[1)] and T.Obiki[2)]

[1)]Faculty of Energy Science, Kyoto University, Uji, Japan

[2)]Institute of Advanced Energy, Kyoto University, Uji, Japan

[3)]National Institute for Fusion Science, Nagoya, Japan

[4)]St.Petersburg Technical University, Russia

[5)]Faculty of Engineering, Kyoto University, Kyoto, Japan

[6)]Interdisciplinary Graduate School of Engineering Science, Kyushu University, Kasuga, Japan

abstract

Li pellet injection has provided a complex plasma with a large fraction of Li ions, which is characterized by intense emissions from Li I and III. The spatial profiles of the fully ionized Li^{3+} ions are measured by charge exchange recombination spectroscopy with a resolution of 13 mm, and the local decay time of the injected Li ion has been estimated. The spectral profile of the charge exchange recombination line of Li^{2+} from n=5 to n=4 shows a complicated structure, which depends on Li^{3+} density. The effects on other intrinsic impurities and recycled Li are also discussed.

Key Words: lithium pellet injection, Heliotron E, charge exchange recombination spectroscopy, impurity particle behavior, spectral profile of Li^{2+} ions,

1. Introduction

Li pellet injection has been recently in producing high performance plasmas [1,2,3]. The ablation mechanism of Li pellet is also of interest because of high sublimation energy compared to hydrogen and deuterium pellets [4,5]. The development of Li pellet injectors and study of the interaction between injected Li and plasma are thus urgent issues for fusion oriented experiments. In Heliotron E [6], a Li-pellet injector has been developed in order to obtain good performance plasmas, to study the ablation mechanisms and to establish a new diagnostic method for the measurement of the magnetic field direction. Injected Li is also used as a tracer for investigating particle transport and for analyzing spectral profiles of Li ions. It is important to study the behavior of the injected Li ions for understanding above subjects.
In this paper, the behavior of the injected Li ions in neutral beam heated plasmas is presented. In paticular fully ionized Li^{3+} ions are measured by a charge exchange recombination spectroscopy, and the local decay time of Li^{3+} is estimated. Effects of Li on intrinsic impurities are also described.

2. Li pellet injector and diagnostics

The Li pellet injector consists of a magazine for pellets, gun barrel, guide tubes and differential pumping system with a buffer tank of 0.1 m^3 [7]. 30 pre-shaped Li pellets 1mm in diameter and length are filled into the holes in the rotatable disk of the magazine. A single pellet has 3.6×10^{19} Li atoms. The gun barrel is 1 m long and 1 mm in diameter. The four guide tubes are 0.14 m, 1.5 m, 0.4 m, and 2.7 m long, respectively. The diameters of these guide tubes are 2.27 mm, 4 mm, 7.53 mm and 10.7 mm, respectively. High pressure He is used as a propellant gas. The injection speed is 400~500 m/s, which is measured between the gun barrel and the first guide tube. The pellet trajectory distributes within a cone of 1 degrees full angle. Pellets are injected horizontally and cross the plasma column nearly perpendicularly. The minor radius of the plasma column is 0.3 m, and the ablation time is 1.3 ms. A high speed camera is used to record images of the ablation cloud at every 50 μs. Two optical filters for Li I (6706 Å) and Li II (5485 Å) are provided to estimate the ablation rates. A multi-channel vacuum ultraviolet spectrometer, which is available from 45Å to 400Å, is used to measure Li III (135 Å) emission. The neutral Li I (6706 Å) emitted near the wall is measured by a visible spectrometer, which is separated by 132 degrees in the toroidal direction from the port of the pellet injector. A 1.26 m visible spectrometer with a 2-dimensional detector

(Hamamatsu,C3554X) [8] is employed to analyze the spectral profiles of the Li^{2+} line populated by charge exchange recombination from Li^{3+} ion. The time resolution is 20 ms. The sight-lines of 40 fiber optics cross the plasma column from 1.98 m to 2.42 m on a major radius and the spatial resolution is 13 mm. The profiles of the electron density and temperature are measured by a Thomson scattering system [9], and ion temperature profile is estimated by the above charge exchange recombination spectroscopy.

3. Behavior of Li ions

A Li pellet is injected into a plasma, which is initiated by a 106GHz gyrotron and further heated by neutral beams of 3.5MW power. The acceleration voltage of the neutral beams is 23 kV. The magnetic field strength is 1.9 T. The vacuum chamber wall has been "boronized" by using an ECH discharge with $B_{10}H_{14}$ and Hc [10]. Figure 1 shows the time evolutions of the average electron density with and without Li pellet. The incremental electron density by pellet injection is also shown. The plasma is produced at 275 ms and the neutral beam heating starts at 300 ms and terminates at 444 ms. After the Li pellet is injected at 327 ms, the average electron density increases by $4\times10^{13}cm^{-3}$. Figure 2 (a) and (b) show the profiles of the electron temperature and density immediately before and after the Li pellet injection. The central electron temperature drops from 0.75 keV to 0.45 keV, and the central electron density increases from 4.5×10^{13} cm^{-3} to 1.4×10^{14} cm^{-3}. The electron energy has almost doubled after the Li pellet injection. The ablation rate of 3.5×10^{22} atoms/s is estimated at the plasma center. In this case, the increase of the electron density is smaller than that provided by fully ablated Li pellet. The injected Li pellet does not completely ablate and about 60% of the pellet is deposited in the plasma. The density ratio of the Li^{3+} ions to protons is estimated to be 0.6, but this ratio decreases rapidly as shown later.

Figure 3 shows spectra in the wavelength region from 170 Å to 400 Å before (320 ms) and after (330 ms) the Li pellet injection. The integration time is 10 ms. The base line is shifted in the upper spectrum. The prominent line is Li III (135 Å), which appears at 270 Å in the second order. The emission of Li II (199.3 Å) is not observed. Other prominent lines originate from intrinsic impurities such as carbon, oxygen, titanium, chromium and iron. Figure 4 shows the time evolution of the Li III, O V(192.9 Å) and Fe XV (284.1 Å) emissions are also shown as typical examples of light and heavy impurities. Immediately after Li pellet injection emission

of Li III peaks and decreases with a decay time of about 60 ms. Similarly a sharp peak appears in Fe XV emission, which increases again from 360 ms to the end of the neutral beam pulse due to continuous influx of iron. Pellet injection causes emission from the high ionization states of metallic impurities to increase significantly, but appears to have a much smaller effect on oxygen and carbon emission. This suggests that the pellet penetrates into the plasma core and iron emission may be enhanced by either an increase in central electron density or by recombination of higher ionization states caused by a drop of the electron temperature.

The fully ionized Li^{3+} ion has been studied using charge exchange recombination spectroscopy. The transition from n=5 to n=4 is selected, the only one available to our diagnostic system. The wavelength from ^2G to ^2F is 4499 Å [11]. Figure 5 shows the intensity profiles of 4499 Å from 370 ms to 450 ms. The horizontal axis is the major radius and the magnetic axis is located at 2.2 m. The Li pellet is injected at 378 ms. The decay time of Li^{3+} is estimated at various locations by exponential fitting from 390 ms to 430 ms. At R=2.2 m, on the magnetic axis, the decay time is 90 ms, and 160 ms is obtained at R=2.1 m and 60 ms at R=2.3 m. There appears an asymmetry between inboard and outboard of the plasma column. This asymmetry is attributed to the slow increase of the penetrated neutral beam density in the inboard due to the decrease in the electron density as described later. The Li III (135 Å), observed by the VUV spectrometer, shows a decrease with a decay time of 60 ms. In this shot the average electron density increased from 2.5×10^{13} cm^{-3} to 9×10^{13} cm^{-3} by the pellet, and then decreased to 7×10^{13} cm^{-3} with a decay time of 160 ms.

Figure 6 shows the spectral profiles of around 4499 Å at sucessive times after the pellet. There appear to be several line components, which are in the wavelength region corresponding to transitions from the n=5 sublevels; ^2P, ^2D, ^2F and ^2G. Arrows in the figure indicate the calculated average wavelengths from designated upper levels. The shorter wavelength components are dominant in the early phase after the Li injection. As Li density decreases, the dominant component shifts to the longer wavelength. This corresponds to the transition from low orbital angular momentum to high orbital angular momentum transitions. The depopulation among the levels due to collision in high density regime is considered as a candidate for the explanation, but there is no similar phenomenon in carbon. In the Li^{3+} ion case, the density is so large it is possible that this depopulation is due to collisions among Li ions.

4. Behavior of the neutral Li line

Neutral Li emission at 6706 Å is used to study the behavior of recycled Li after the Li pellet injection. A spectrometer with a focal length of 1.26 m and a 1024 channel diode array detector is used. The time resolution is 10 ms. Figure 7 shows the shot-to-shot variations of Li I intensity. Li shots are denoted by closed circles and open squares correspond to shots without a pellet. The neutral beam power is 3.2~3.4 MW. For the shots with pellet the intensities are estimated at the time before the Li pellet is injected. The Li I emission is again visible from shots following pellet injection shots indicating Li recycling. Injection of Li pellets in successive shots can cause a cumulative increase in Li I emission and a gradual fall in Li I emission can be seen one to two shots after Li pellet injection has ceased. When corrected for differences in electron density, the shot-to-shot decay of Li I density appears to be exponential. Oxygen is an interesting impurity in pellet injected shots. The intensity typically decreases in successive shots, but no reduction in the relative impurity level normalized by the electron density is observed.

5. Conclusion

In Heliotron E, a Li pellet injector with good reproducibility and reliability has been developed and successfully injected into neutral beam heated plasmas. The spatial profiles of the Li III emission from Li^{3+} are measured with a resolution of 13 mm, and local decay time is estimated. This diagnostic method can be used to estimate the local values. Moreover the emission intensity is determined only by the product of neutral beam and Li^{3+} densities so complicated analysis on excitation and ionization is not necessary. The fine structure from sublevels of the charge exchange recombination line from n=5 to n=4 is analyzed. The collision among Li ions is considered to be the most probable candidate for the depopulation.

Acknowledgment

The authors are grateful to the Heliotron group for their excellent and helpful support. The authors would like to thank Dr. J. Terry for critical reading of the manuscript.

References

[1] J.L.Terry et al., 13th IAEA Washington, 1990, vol.1, 393

[2] J.A.Snipes, E.S.Marmar, J.L.Terry et al.J. Nucl.Mater. 196-198 (1992) 686

[3] B.V.Kuteev, V.Yu. Sergeev, L.D.Tsendin,Sov.J.Plasma Phys. 10 (1984) 675

[4] P.B.Parks, J.S.Leffler, R.K.Fisher, Nuclear Fusion 28 (1988) 477

[5] T. Obiki et al., 15th Int.Conf.on Plasma Physics and Controlled Nuclear Fusion Research, Seville, 1994,(IAEA, Vienna, 1995) Vol.I,p757

[6] K.V.Khlopenkov, V.Yu.Sergeev, S.Sudo et al., 7th Int.Conf.on Plasma Physics and Controlled Nuclear Fusion, Toki, Japan, 1995

[7] K.Ida and S.Hidekuma, Rev.Sci.Instrum., 60 (1989) 867

[8] H.Funaba, H.Okada et al., 7th Int.Conf.on Plasma Physics and Controlled Nuclear Fusion, Toki, Japan, 1995

[9] K.Kondo, T.Mizuuchi, et al., J.Nucl.Mater. 220-222(1995) 1052

[10] S.Bashkin and J.O.Stoner, Atomic Energy Levels and Grotrian Diagrams I, North-Holland Pub.Co. Amsterdam,1975

Figure captions

Fig.1

The time evolutions of the average electron densities. The solid line is for the shot with Li pellet injection at 336 ms and the dotted line corresponds to the shot without pellet injection. The incremental density by pellet injection is also plotted.

Fig.2

The electron temperature (a) and density (b) profiles immediately before(closed) and after(open) the pellet injection.

Fig.3

The spectra in the vacuum ultraviolet region before and after the pellet injection. Li III(135 Å) appears at 270 Å in second order.

Fig.4

The time evolutions of the intensities of Li III, O V and Fe XV.

Fig.5

Spatial profiles of Li^{2+} emissions measured by charge exchange recombination spectroscopy. Li pellet is injected at 376 ms.

Fig.6

Spectral profiles of charge exchange recombination line from n=5 to n=4 transition. Arrows indicate the calculated average wavelengths from designated upper levels.

Fig.7

Li I intensity in successive shots with and without Li pellets. Closed circles are with Li pellet injection and open squares are without.

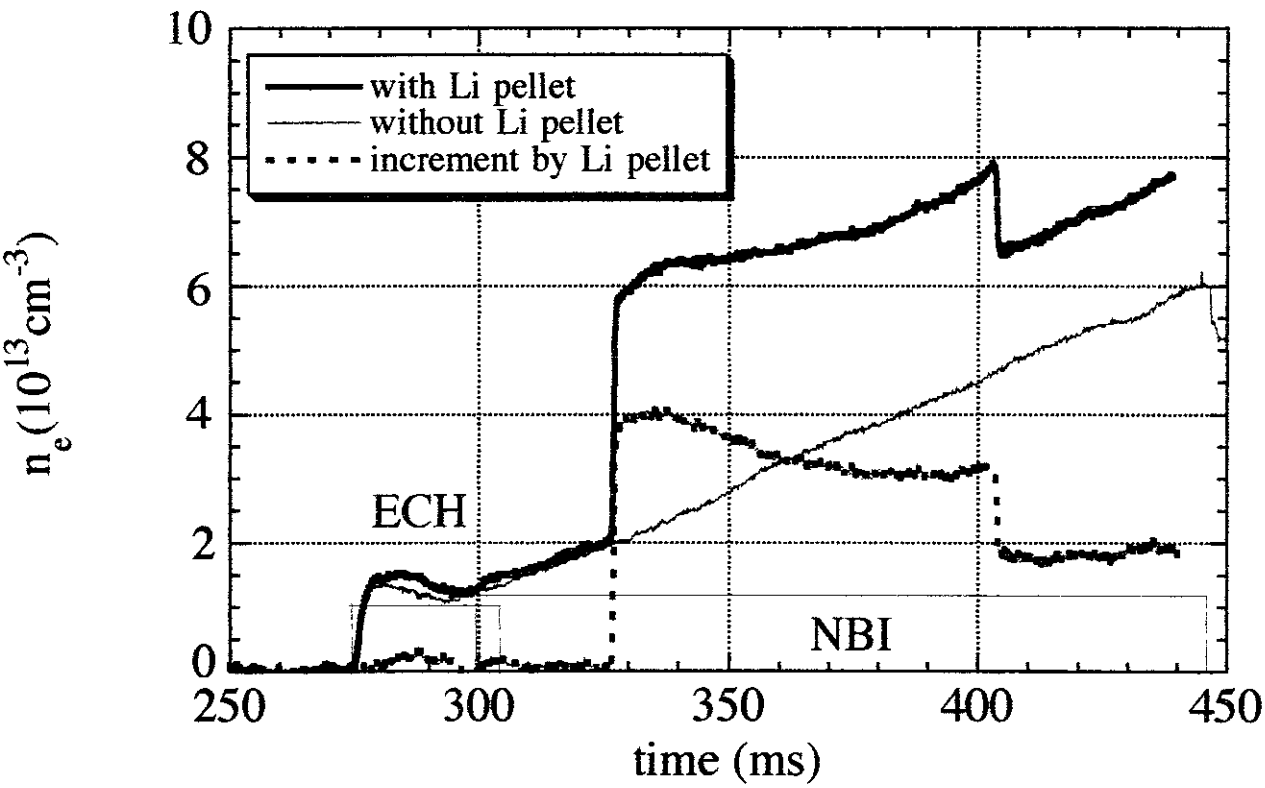
10
8
6
4
2
0
250
300
350
400
450
time (ms)
$n_e(10^{13}cm^{-3})$
with Li pellet
without Li pellet
increment by Li pellet
ECH
NBI

Fig.1

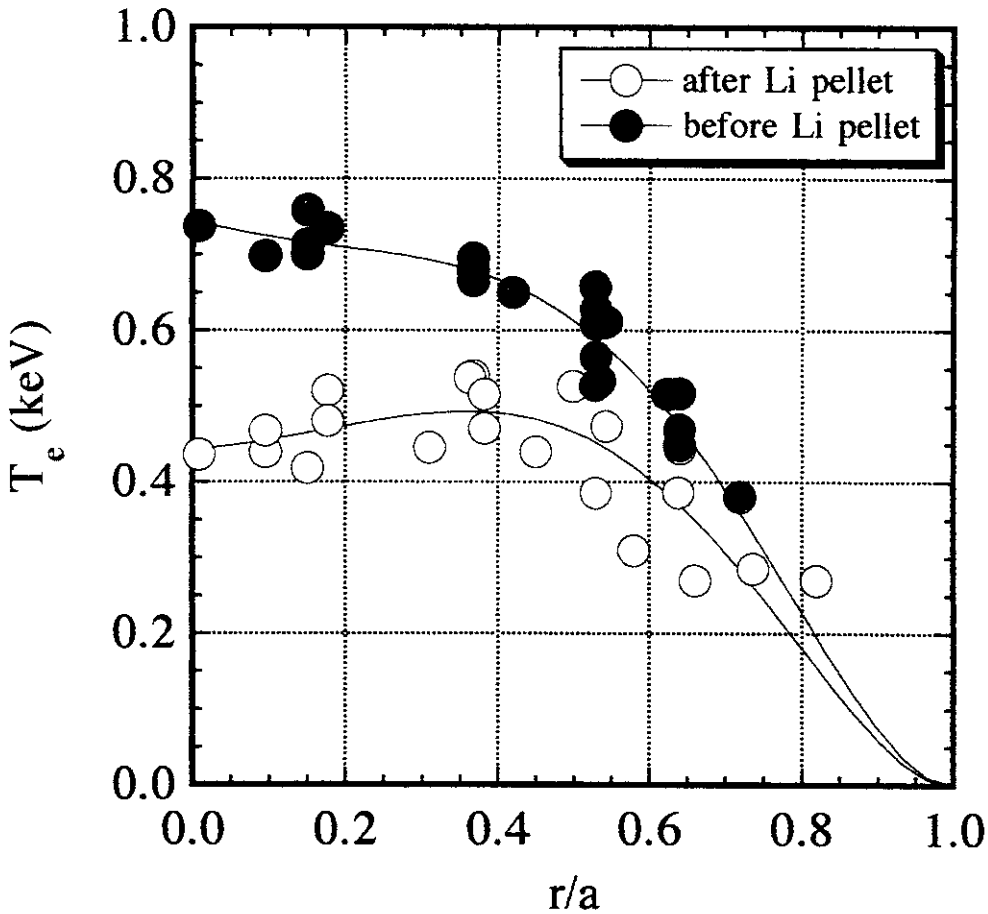
1.0
0.8
0.6
0.4
0.2
0.0
T_e (keV)
0.0
0.2
0.4
0.6
0.8
1.0
r/a
after Li pellet
before Li pellet

Fig.2(a)

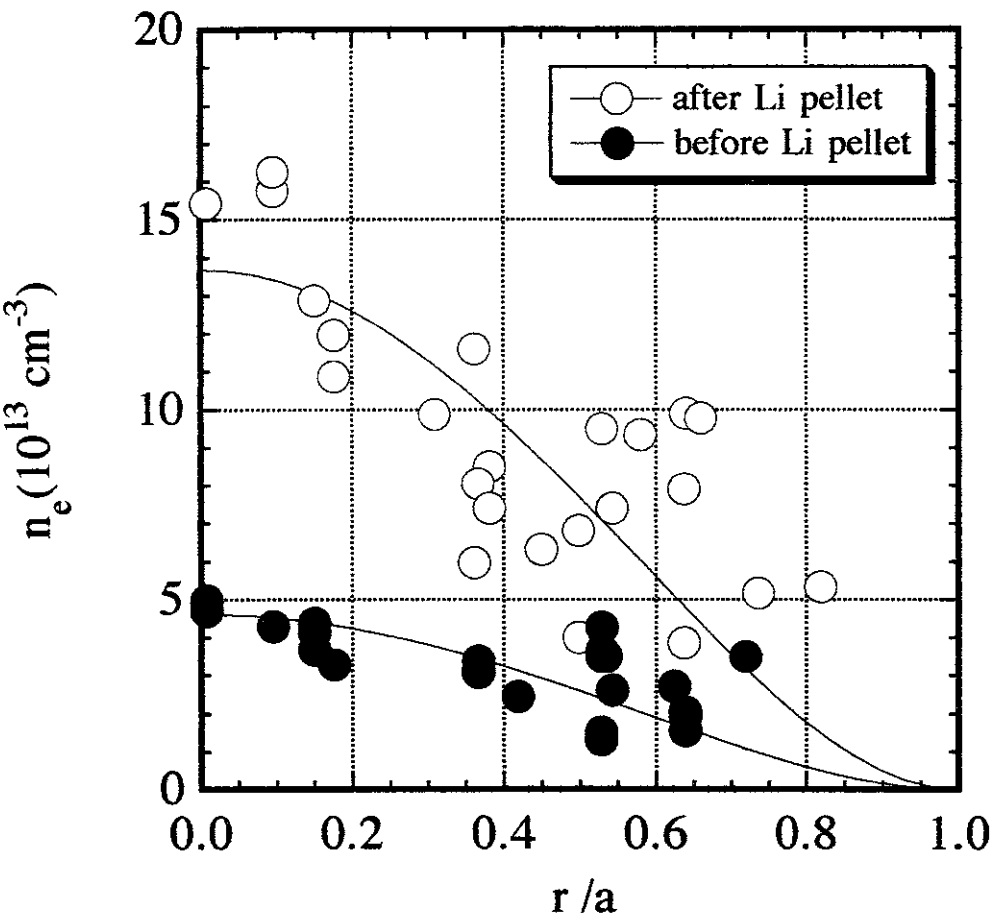
20
15
10
5
0
0.0
0.2
0.4
0.6
0.8
1.0
r /a
$n_e(10^{13}\ cm^{-3})$
after Li pellet
before Li pellet

Fig.2(b)

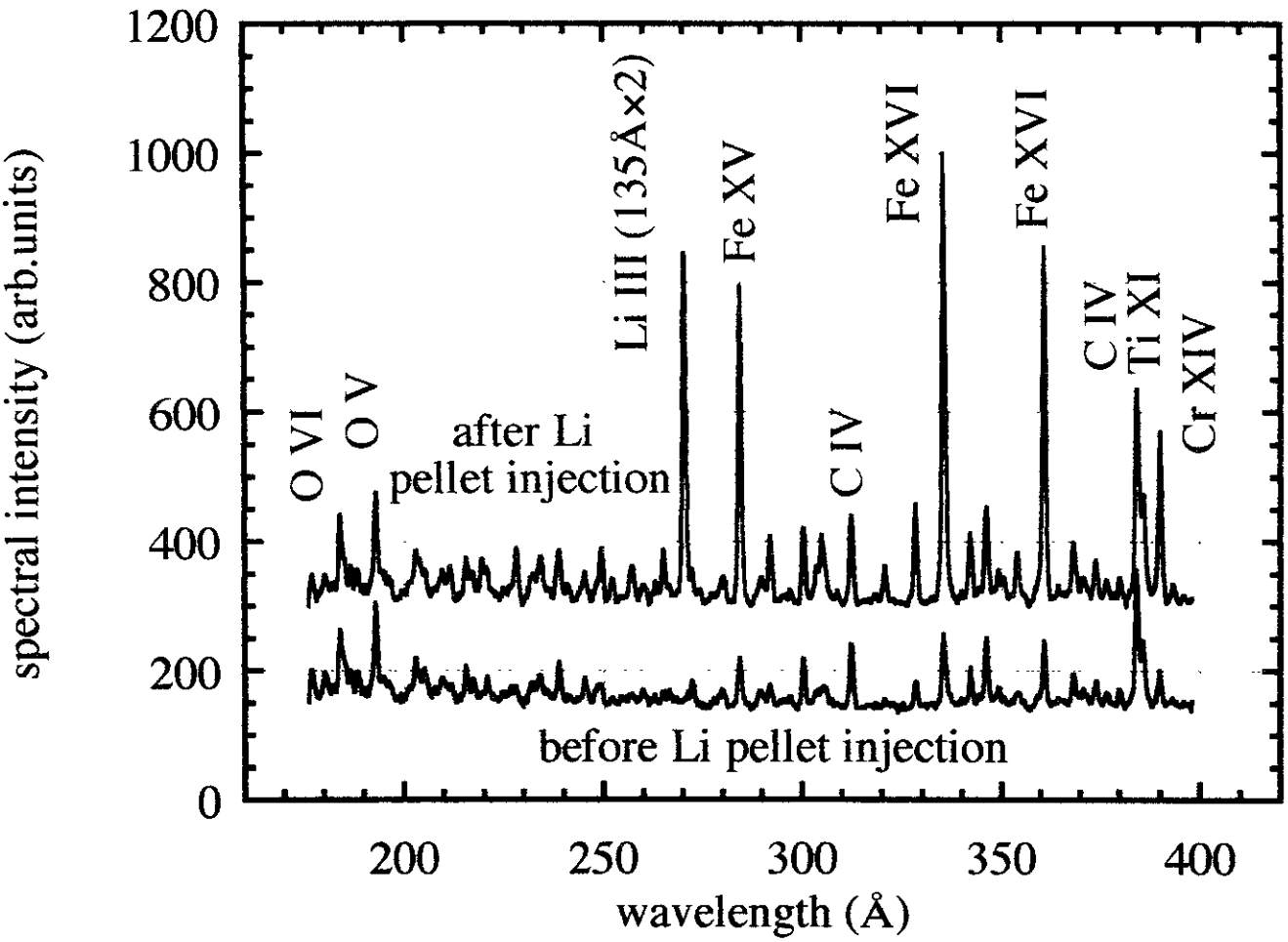
spectral intensity (arb.units)
1200
1000
800
600
400
200
0
200
250
300
350
400
wavelength (Å)
O VI
O V
after Li
pellet injection
Li III (135Å×2)
Fe XV
C IV
Fe XVI
Fe XVI
C IV
Ti XI
Cr XIV
before Li pellet injection

Fig.3

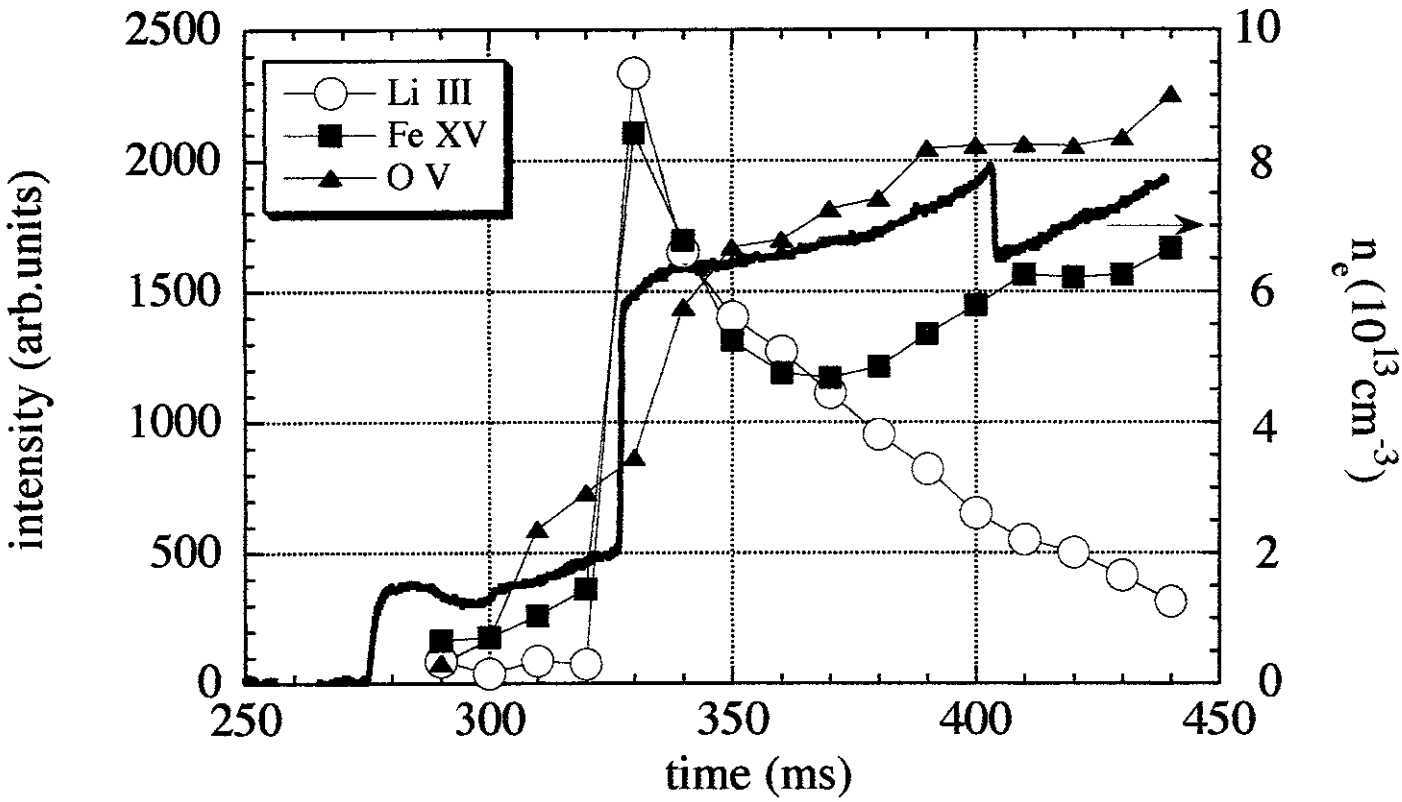
Li III
Fe XV
O V
intensity (arb.units)
$n_e(10^{13}cm^{-3})$
time (ms)
2500
2000
1500
1000
500
0
10
8
6
4
2
0
250
300
350
400
450

Fig.4

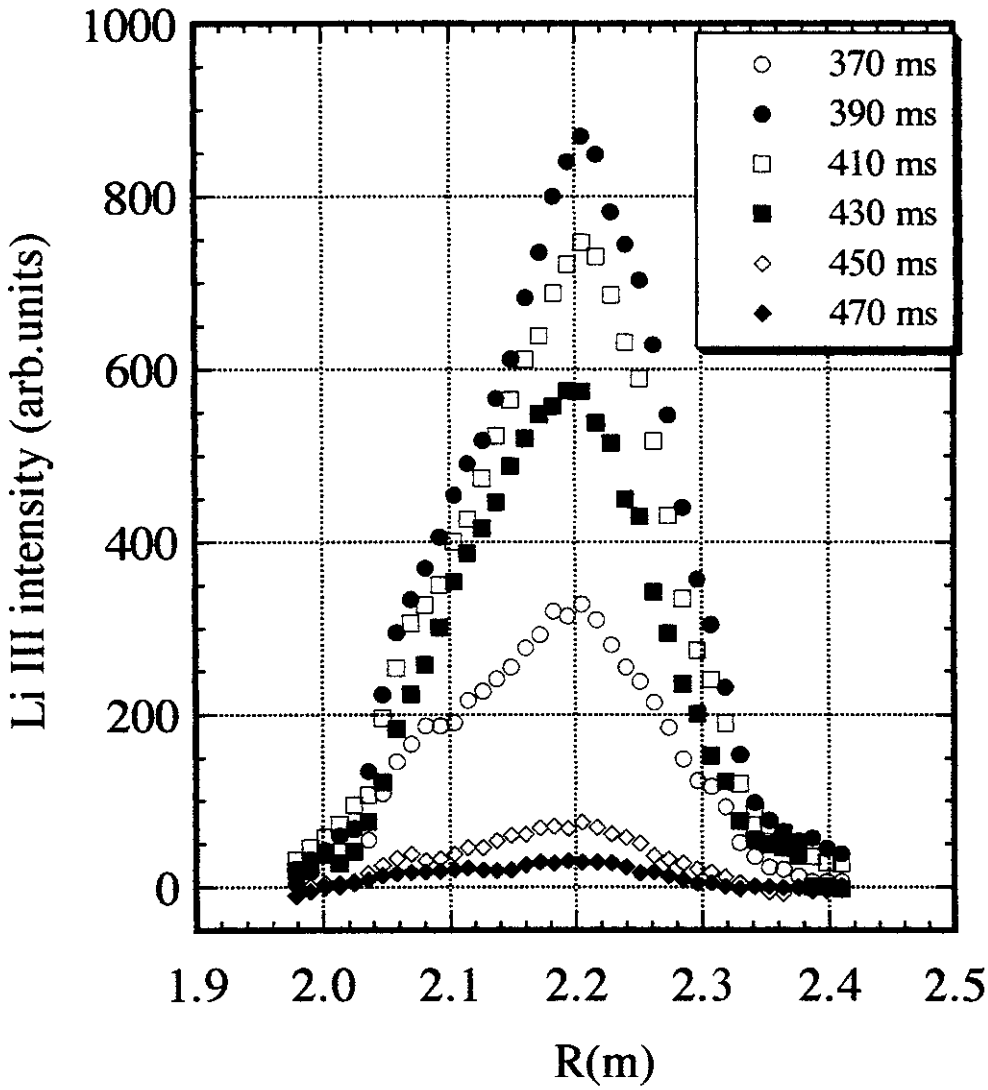
1000
800
600
400
200
0
Li III intensity (arb.units)
1.9
2.0
2.1
2.2
2.3
2.4
2.5
R(m)
370 ms
390 ms
410 ms
430 ms
450 ms
470 ms

Fig.5

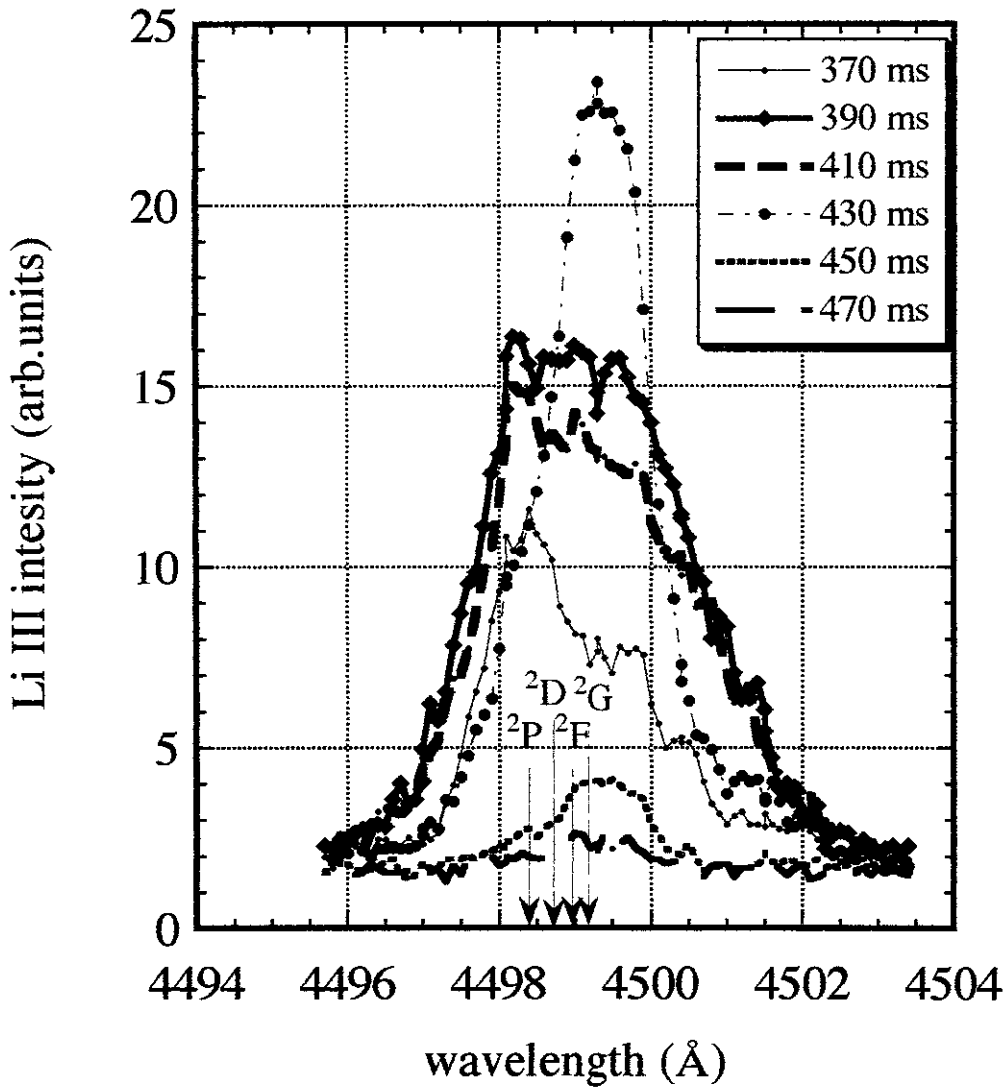
25
20
15
10
5
0
4494
4496
4498
4500
4502
4504
Li III intesity (arb.units)
wavelength (Å)
370 ms
390 ms
410 ms
430 ms
450 ms
470 ms
^{2}D ^{2}G
^{2}P ^{2}F

Fig.6

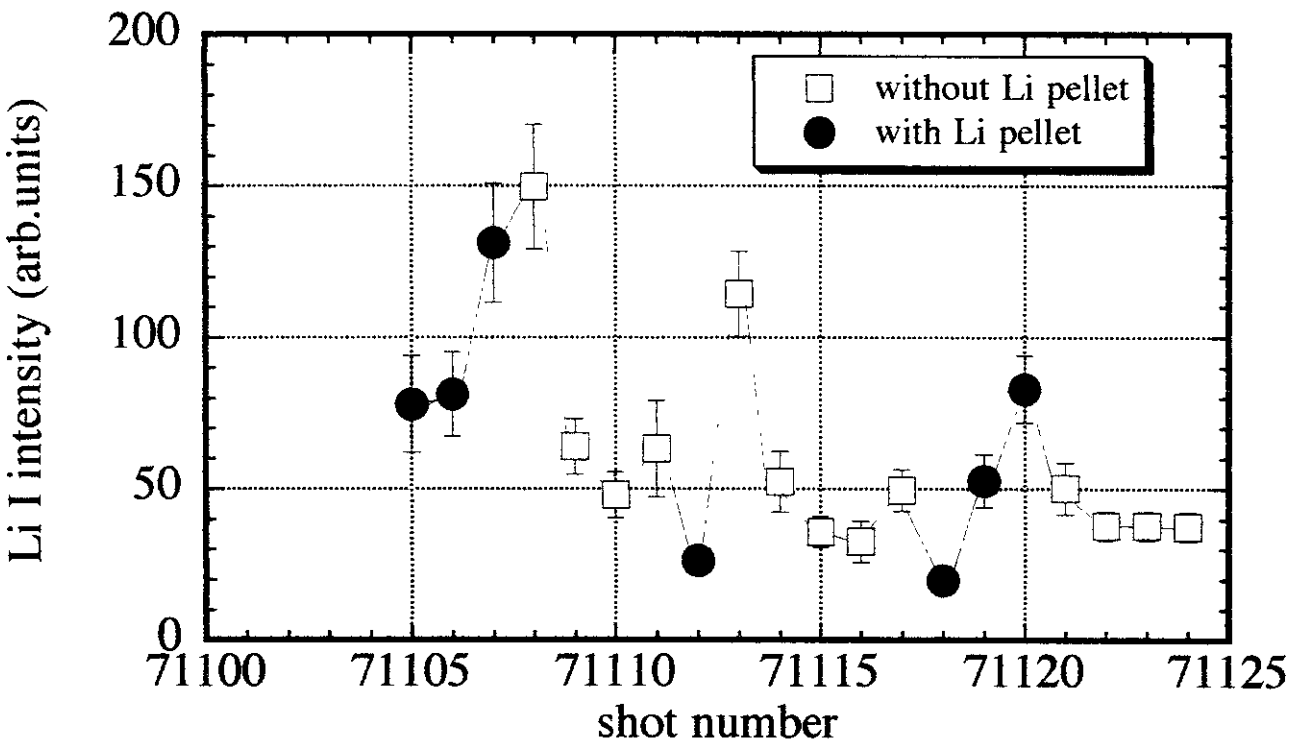
200
150
100
50
0
Li I intensity (arb.units)
71100
71105
71110
71115
71120
71125
shot number
without Li pellet
with Li pellet

Fig.7

Recent Issues of NIFS Series

NIFS-375 U. Stroth, M. Murakami, R.A. Dory, H. Yamada, S. Okamura, F. Sano and T. Obiki,
Energy Confinement Scaling from the International Stellarator Database; Sep. 1995

NIFS-376 S. Bazdenkov, T. Sato, K. Watanabe and The Complexity Simulation Group,
Multi-Scale Semi-Ideal Magnetohydrodynamics of a Tokamak Plasma; Sep. 1995

NIFS-377 J. Uramoto,
Extraction of Negative Pionlike Particles from a H2 or D2 Gas Discharge Plasma in Magnetic Field; Sep. 1995

NIFS-378 K. Akaishi,
Theoretical Consideration for the Outgassing Characteristics of an Unbaked Vacuum System; Oct. 1995

NIFS-379 H. Shimazu, S. Machida and M. Tanaka,
Macro-Particle Simulation of Collisionless Parallel Shocks; Oct. 1995

NIFS-380 N. Kondo and Y. Kondoh,
Eigenfunction Spectrum Analysis for Self-organization in Dissipative Solitons; Oct. 1995

NIFS-381 Y. Kondoh, M. Yoshizawa, A. Nakano and T. Yabe,
Self-organization of Two-dimensional Incompressible Viscous Flow in a Friction-free Box; Oct. 1995

NIFS-382 Y.N. Nejoh and H. Sanuki,
The Effects of the Beam and Ion Temperatures on Ion-Acoustic Waves in an Electron Beam-Plasma System; Oct. 1995

NIFS-383 K. Ichiguchi, O. Motojima, K. Yamazaki, N. Nakajima and M. Okamoto
Flexibility of LHD Configuration with Multi-Layer Helical Coils; Nov. 1995

NIFS-384 D. Biskamp, E. Schwarz and J.F. Drake,
Two-dimensional Electron Magnetohydrodynamic Turbulence; Nov. 1995

NIFS-385 H. Kitabata, T. Hayashi, T. Sato and Complexity Simulation Group,
Impulsive Nature in Collisional Driven Reconnection; Nov. 1995

NIFS-386 Y. Katoh, T. Muroga, A. Kohyama, R.E. Stoller, C. Namba and O. Motojima,
Rate Theory Modeling of Defect Evolution under Cascade Damage Conditions:The Influence of Vacancy-type Cascade Remnants and Application to the Defect Production Chracterization by Microstructural

Analysis; Nov. 1995

NIFS-387 K. Araki, S. Yanase and J. Mizushima,
Symmetry Breaking by Differential Rotation and Saddle-node Bifurcation of the Thermal Convection in a Spherical Shell; Dec. 1995

NIFS-388 V.D. Pustovitov,
Control of Pfirsch-Schlüter Current by External Poloidal Magnetic Field in Conventional Stellarators: Dec. 1995

NIFS-389 K. Akaishi,
On the Outgassing Rate Versus Time Characteristics in the Pump-down of an Unbaked Vacuum System; Dec. 1995

NIFS-390 K.N. Sato, S. Murakami, N. Nakajima, K. Itoh,
Possibility of Simulation Experiments for Fast Particle Physics in Large Helical Device (LHD); Dec. 1995

NIFS-391 W.X.Wang, M. Okamoto, N. Nakajima, S. Murakami and N. Ohyabu,
A Monte Carlo Simulation Model for the Steady-State Plasma in the Scrape-off Layer; Dec. 1995

NIFS-392 Shao-ping Zhu, R. Horiuchi, T. Sato and The Complexity Simulation Group,
Self-organization Process of a Magnetohydrodynamic Plasma in the Presence of Thermal Conduction; Dec. 1995

NIFS-393 M. Ozaki, T. Sato, R. Horiuchi and the Complexity Simulation Group
Electromagnetic Instability and Anomalous Resistivity in a Magnetic Neutral Sheet; Dec. 1995

NIFS-394 K. Itoh, S.-I Itoh, M. Yagi and A. Fukuyama,
Subcritical Excitation of Plasma Turbulence; Jan. 1996

NIFS-395 H. Sugama and M. Okamoto, W. Horton and M. Wakatani,
Transport Processes and Entropy Production in Toroidal Plasmas with Gyrokinetic Eletromagnetic Turbulence; Jan. 1996

NIFS-396 T. Kato, T. Fujiwara and Y. Hanaoka,
X-ray Spectral Analysis of Yohkoh BCS Data on Sep. 6 1992 Flares - Blue Shift Component and Ion Abundances -; Feb. 1996

NIFS-397 H. Kuramoto, N. Hiraki, S. Moriyama, K. Toi, K. Sato, K. Narihara, A. Ejiri, T. Seki and JIPP T-IIU Group,
Measurement of the Poloidal Magnetic Field Profile with High Time Resolution Zeeman Polarimeter in the JIPP T-IIU Tokamak; Feb. 1996

NIFS-398 J.F. Wang, T. Amano, Y. Ogawa, N. Inoue,
Simulation of Burning Plasma Dynamics in ITER; Feb. 1996

NIFS-399 K. Itoh, S-I. Itoh, A. Fukuyama and M. Yagi,
Theory of Self-Sustained Turbulence in Confined Plasmas; Feb. 1996

NIFS-400 J. Uramoto,
A Detection Method of Negative Pionlike Particles from a H2 Gas Descharge Plasma; Feb. 1996

NIFS-401 K.Ida, J.Xu, K.N.Sato, H.Sakakita and JIPP TII-U group,
Fast Charge Exchange Spectroscopy Using a Fabry-Perot Spectrometer in the JIPP TII-U Tokamak; Feb. 1996

NIFS-402 T. Amano,
Passive Shut-Down of ITER Plasma by Be Evaporation; Feb. 1996

NIFS-403 K. Orito,
A New Variable Transformation Technique for the Nonlinear Drift Vortex; Feb. 1996

NIFS-404 T. Oike, K. Kitachi, S. Ohdachi, K. Toi, S. Sakakibara, S. Morita, T. Morisaki, H. Suzuki, S. Okamura, K. Matsuoka and CHS group; *Measurement of Magnetic Field Fluctuations near Plasma Edge with Movable Magnetic Probe Array in the CHS Heliotron/Torsatron*; Mar. 1996

NIFS-405 S.K. Guharay, K. Tsumori, M. Hamabe, Y. Takeiri, O. Kaneko, T. Kuroda,
Simple Emittance Measurement of H- Beams from a Large Plasma Source; Mar. 1996

NIFS-406 M. Tanaka and D. Biskamp,
Symmetry-Breaking due to Parallel Electron Motion and Resultant Scaling in Collisionless Magnetic Reconnection; Mar. 1996

NIFS-407 K. Kitachi, T. Oike, S. Ohdachi, K. Toi, R. Akiyama, A. Ejiri, Y. Hamada, H.Kuramoto, K. Narihara, T. Seki and JIPP T-IIU Group,
Measurement of Magnetic Field Fluctuations within Last Closed Flux Surface with Movable Magnetic Probe Array in the JIPP T-IIU Tokamak; Mar. 1996

NIFS-408 K. Hirose, S. Saito and Yoshi.H. Ichikawa
Structure of Period-2 Step-1 Accelerator Island in Area Preserving Maps; Mar. 1996

NIFS-409 G.Y.Yu, M. Okamoto, H. Sanuki, T. Amano,
Effect of Plasma Inertia on Vertical Displacement Instability in Tokamaks; Mar. 1996

NIFS-410 T. Yamagishi,
Solution of Initial Value Problem of Gyro-Kinetic Equation; Mar. 1996

NIFS-411 K. Ida and N. Nakajima,
Comparison of Parallel Viscosity with Neoclassical Theory; Apr. 1996

NIFS-412 T. Ohkawa and H. Ohkawa,
Cuspher, A Combined Confinement System; Apr. 1996

NIFS-413 Y. Nomura, Y.H. Ichikawa and A.T. Filippov,
Stochasticity in the Josephson Map; Apr. 1996

NIFS-414 J. Uramoto,
Production Mechanism of Negative Pionlike Particles in H_2 Gas Discharge Plasma; Apr. 1996

NIFS-415 A. Fujisawa, H. Iguchi, S. Lee, T.P. Crowley, Y. Hamada, S. Hidekuma, M. Kojima,
Active Trajectory Control for a Heavy Ion Beam Probe on the Compact Helical System; May 1996

NIFS-416 M. Iwase, K. Ohkubo, S. Kubo and H. Idei
Band Rejection Filter for Measurement of Electron Cyclotron Emission during Electron Cyclotron Heating; May 1996

NIFS-417 T. Yabe, H. Daido,T. Aoki, E. Matsunaga and K. Arisawa,
Anomalous Crater Formation in Pulsed-Laser-Illuminated Aluminum Slab and Debris Distribution; May 1996

NIFS-418 J. Uramoto,
Extraction of K^- Mesonlike Particles from a D_2 Gas Discharge Plasma in Magnetic Field; May 1996

NIFS-419 J. Xu, K. Toi, H. Kuramoto, A. Nishizawa, J. Fujita, A. Ejiri, K. Narihara, T. Seki, H. Sakakita, K. Kawahata, K. Ida, K. Adachi, R. Akiyama, Y. Hamada, S. Hirokura, Y. Kawasumi, M. Kojima, I. Nomura, S. Ohdachi, K.N. Sato
Measurement of Internal Magnetic Field with Motional Stark Polarimetry in Current Ramp-Up Experiments of JIPP T-IIU; June 1996

NIFS-420 Y.N. Nejoh,
Arbitrary Amplitude Ion-acoustic Waves in a Relativistic Electron-beam Plasma System; July 1996

NIFS-421 K. Kondo, K. Ida, C. Christou, V.Yu.Sergeev, K.V.Khlopenkov, S.Sudo, F. Sano, H. Zushi, T. Mizuuchi, S. Besshou, H. Okada, K. Nagasaki, K. Sakamoto, Y. Kurimoto, H. Funaba, T. Hamada, T. Kinoshita, S. Kado, Y. Kanda, T. Okamoto, M. Wakatani and T. Obiki,
Behavior of Pellet Injected Li Ions into Heliotron E Plasmas; July 1996